Characterization of Pure and Doped ZnO Nanostructured Powders elaborated in Solar Reactor

Adriana-Gabriela Schiopu
Pitesti University Centre, Faculty of Mechanics and Technology, Politehnica Bucharest National University of Science and Technology, Romania
gabriela.schiopu@upb.ro

Mihai Oproescu
Pitesti University Centre, Faculty of Mechanics and Technology, Politehnica Bucharest National University of Science and Technology, Romania
mihai.oproescu@upb.ro (corresponding author)

Vasile Gabriela Iana
Pitesti University Centre, Faculty of Mechanics and Technology, Politehnica Bucharest National University of Science and Technology, Romania
vasile_gabriel.iana@upb.ro

Sorin Georgian Moga
Pitesti University Centre, Regional Center of Research and Development for Materials, Processes and Innovative Products Dedicated to the Automotive Industry, Politehnica Bucharest National University of Science and Technology, Romania
sorin_georgian.moga@upb.ro

Denis Aurelian Negrea
Pitesti University Centre, Regional Center of Research and Development for Materials, Processes and Innovative Products Dedicated to the Automotive Industry, Politehnica Bucharest National University of Science and Technology, Romania
aurelian.negrea@upb.ro

Denisa Stefania Vilcoci
Pitesti University Centre, Regional Center of Research and Development for Materials, Processes and Innovative Products Dedicated to the Automotive Industry, Politehnica Bucharest National University of Science and Technology, Romania
denisa.vilcoci@upb.ro

Georgiana Cirstea
Pitesti University Centre, Regional Center of Research and Development for Materials, Processes and Innovative Products Dedicated to the Automotive Industry, Politehnica Bucharest National University of Science and Technology, Romania
georgiana.cirstea93@upb.ro

Catalin Marian Ducu
Pitesti University Centre, Regional Center of Research and Development for Materials, Processes and Innovative Products Dedicated to the Automotive Industry, Politehnica Bucharest National University of

Science and Technology, Romania
marian_catalin.ducu@upb.ro

Miruna-Adriana Iota
Doctoral School Materials Science and Engineering, National University of Science and Technology Politehnica Bucharest | National R&D Institute for Non-Ferrous and Rare Metals, INCDMNR-IMNR, 102 Biruintei Blvd, 077145 Pantelimon, Romania
iota.miruna@imnr.ro

Received: 17 January 2024 | Revised: 5 February 2024 | Accepted: 18 February 2024

 DOI: https://doi.org/10.48084/etasr.6923

ABSTRACT

The synthesis of nano-oxides is an important field of nanotechnology, as these materials possess unique properties and applications. Several methods have been developed for synthesizing nano-oxides, each offering advantages and disadvantages depending on the desired material characteristics. Solar energy focused on solar reactors can be utilized for nano-oxide elaboration, offering a sustainable and environmentally friendly approach. The current article presents the research carried out for the elaboration of pure and doped nanostructured zinc oxides using solar energy. The morphostructural characteristics were determined by X-Ray Diffraction (XRD), Scanning Electron Microscopy (SEM), and the Brunauer-Emmett-Teller method. The attenuated total reflectance Fourier transform infrared spectroscopy confirmed the synthesis of pure and doped nanostructured ZnO. The optical properties were highlighted by UV-VIS Spectroscopy. The research points out that crystallite sizes vary between 37 and 51 nm due to the influence of doping metal. The morphology associated with these particles is predominantly whiskers with elongated parts between 0.18 and 1.4 um. Doping with Fe, Si, Yb, and Ce causes a wider band gap compared to pure ZnO nanoparticles. As solar energy becomes more accessible and efficient, solar-driven synthesis of pure and doped ZnO is poised to be a crucial factor in shaping the future of material science and technology.

Keywords-zinc oxide; nanostructured; morphology; characterization; solar reactor

I. INTRODUCTION

Solar energy is a sustainable energy source, offering several advantages over conventional energy sources like fossil fuels. Solar energy is derived from the sun's radiant energy, a virtually limitless resource. Unlike fossil fuels, which are finite and will be eventually depleted, solar energy can be harnessed indefinitely [1]. Solar energy can be harnessed in various forms, from rooftop solar panels to large-scale solar farms, making it adaptable to different locations and power requirements [2]. This versatility allows for the integration of solar energy into various energy systems. The field of solar synthesis, which utilizes solar energy to produce materials, has witnessed significant advancements in recent years, leading to the development of novel materials with unique properties and broader applications [3, 4]. These advancements hold immense potential for enhancing the performance and sustainability of solar energy technologies [5]. One notable area of innovation lies in the synthesis of nanomaterials utilizing solar energy. Solar energy offers several advantages over traditional synthesis methods, including:

- Sustainability: Solar energy is a renewable, clean, and abundant energy source [6], making it a more sustainable approach to nanomaterial synthesis compared to energy-intensive methods that rely on fossil fuels or hazardous chemicals [7].
- Efficiency: Solar-driven synthesis processes can be more efficient than conventional methods in terms of energy consumption and waste generation [8, 9].
- Control over size and shape: Solar energy can be used to control the size and shape of nanomaterials more precisely, leading to enhanced properties and applications [10].
- Green chemistry: Solar-based synthesis methods can minimize the use of hazardous chemicals and solvents, reducing the environmental impact of nanomaterials production [11-14].

Solar synthesis techniques enable the production of these nanomaterials with high purity and crystallinity, enhancing their photocatalytic activity. Solar synthesis methods can be employed to synthesize materials with controlled size, morphology, and surface chemistry, tailoring their properties for specific applications [15-23]. In addition to the synthesis of nanomaterials, solar synthesis has also been explored to produce other materials such as $Bi1.7Pb0.3Sr2Ca(n-1)Cu_nO_y$ ($n = 3 \div 5$) ceramics [4].

The choice of the synthesis method depends on the desired specific properties of the nano-oxide, such as particle size, morphology, composition, and crystallinity. ZnO doped nanoparticles can be synthesized using various methods, including sol-gel, co-precipitation, hydrothermal, green synthesis, and Chemical Vapor Deposition (CVD) [24-27]. The choice of thre synthesis method depends on the desired particle

size, morphology, and doping level. For instance, sol-gel methods are well-suited for obtaining uniform and small-sized ZnO NP (nanoparticles), while hydrothermal synthesis can produce larger particles with high crystallinity.

The use of solar energy for pure and doped ZnO nanostructured powder synthesis is an emerging field with the potential to revolutionize the way we produce nanomaterials for various applications. Pure ZnO, $Zn_{1-x}Al_xO$, $Zn_{1-x}In_xO$, $Zn_{1-x}Co_xO$, $Zn_{1-x}Bi_x$, metallic Zn nanophases, nanophases of Si and SiO_x, CuO and Mn-doped CuO,as well as pure TiO_2 and Fe, Co or Mn-doped TiO_2 have been prepared by this method [10, 18]. Processing in a solar reactor has the advantages of giving a physical approach rather a chemical one with the strength of the absence of solvent contamination and the uniformity of nanoparticle distribution.

II. MATERIALS AND METHODS

Solar energy can be used to evaporate metal oxide precursors, leading to the formation of nanoparticles. The method is simple, scalable, and energy efficient, making it suitable for production of nano-oxide powders. The sun can be used to heat solid precursors in specially designed solar reactors. Such reactors are built in the CNRS-PROMES laboratory, UPR 8521, a member of the CNRS (French National Centre for Scientific Research) [28]. The acquired research uses as precursors micrometric oxides, easily procured commercially (Sigma Aldrich, p.a.). Doping was achieved for each dopant element through mechanosynthesis starting from metal oxides M_xO_y (M=Mg, Fe, Si, Ce, Yb), in a proportion of 0.1%, in weight percentage. Inside the solar reactor, the pure and doped ZnO in the form of tablets, is placed on a continuously cooled support. The solar energy captured by mirrors, located on the laboratory's 1st level, is directed to a spherical mirror, on the 6th level of the laboratory [28].

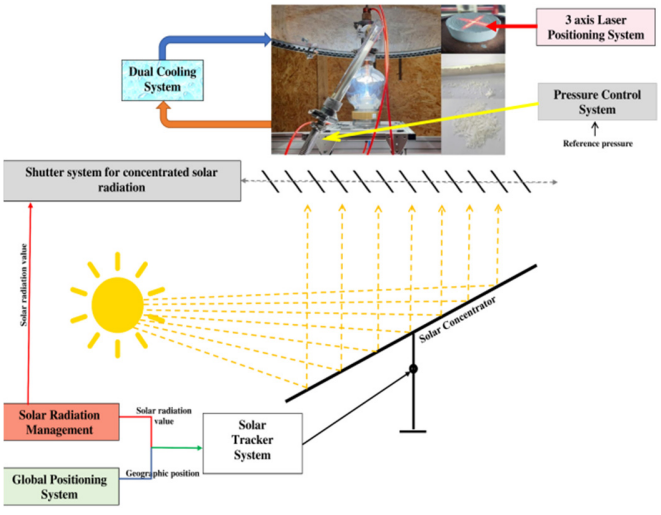

Fig. 1. Production of nanostructured powders in the reactor.

The role of the mirror is to concentrate the solar energy, directed towards the raw tablet. Before the experiment starts, the position of the tablet is verified with a laser beam. Concentrated energy from mirror produces ultra-fast (2-3 min) evaporation. The evaporated particles are driven, due to the pressure in the reactor, to a nanoporous ceramic filter. Their rapid condensation on filter leads to the formation of nanostructured powders. The quantity of elaborated powders depends on the vapor pressure of the material. When the vapor pressure on the top of the melted material is low, the nanopowder quantity is less than 10 g/hour at flux higher than 1 kW/m^2). It is one of the reasons why when larger quantities are needed, a requirement is to associate ball milling with solar elaboration. The entire reactor is semi-automated. The position of the sun and its trajectory are obtained based on the Global Positioning System (GPS) and positioning maps. The Solar Tracker System positions the concentrator plane mirrors, on the laboratory level, to obtain the maximum available solar flux. The target in the center of the reactor core is positioned with the support of the 3 axis Laser Positioning System. The Pressure Control System (implemented with a controlled vacuum pump) maintains the desired pressure in the reactor. The Shutter system is activated by means of an electric motor to assure the solar flux on the spheric mirror. The process parameters are detailed in Table I.

TABLE I. PROCESS PARAMETERS

Sample	Solar flux (W/m^2)	Pressure (mbar)
NP/ZnO	950	300
NP/Mg/ZnO	924	300
NP/Fe/ZnO	750	300
NP/Si/ZnO	910	300
NP/Yb/ZnO	924	300
NP/Ce/ZnO	800	300

The purity of phase is determined by XRD using a Rigaku Ultima IV diffractometer, in Bragg–Brentano geometry. The acquisition parameters were: CuKα radiation (45 kV, λ = 0.154 A°, and 40 mA) and a D/teX Ultra one-dimensional detector with graphite monochromator. SEM by Hitachi SU 8230 Electron Microscope allowed identifying the morphologies. The ATR-FTIR spectra of all powders were recorded with a multireflexion ATR sensor of Bruker Fourier transmission infrared spectrometer, Tensor 27, in the range of 300 to 4000 cm^{-1}, at 4 cm^{-1} resolution. This method is particularly well-suited for analyzing nanoparticles, as it eliminates the need for sample preparation and allows for in situ studies. The powders were analyzed with Micromeritics® TriStar II Plus in a nitrogen atmosphere (absorption-desorption isotherms at 77 K) to determine the specific surface area. The moisture content of the samples was removed by degassing/drying at 300^{0}C for approximately 3 hours before analysis. The optical properties of the particles were studied using UV-Visible spectroscopy by Ocean Optics HR2000+.

III. RESULTS AND DISCUTION

A. Structural Characterization

The crystallinity and the phases of the as-elaborated pure and doped samples were investigated by XRD. Phase analysis of the nanoparticles was conducted in the 2θ range of [25–101°] at a step of 0.05° and a scan speed of 2°/min. The ICDD PDF4+ 2022 database was used for crystalline phase identification [29-34]. The patterns are shown in Figures 3-5.

The diffraction peaks indicate that the particles of pure and Mg, Fe, Si, and Yb-doped ZnO powders present only ZnO peaks corresponding to the P63mc space group [34]. No other impure phases were obtained.

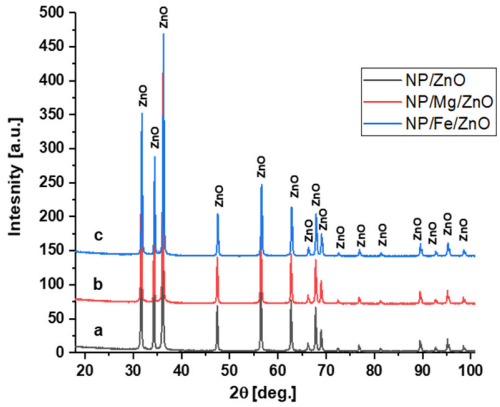

Fig. 2. XRD patterns of the: pure and Mg- and Fe-doped ZnO.

Only in the Ce-doped sample CeO_2 phase, the 225: Fm-3m space group is identified in the XRD spectrum, as shown in Figure 4. The crystallite mean size is determined with Whole-Powder-Pattern Fitting (WPPF) using Pdxl2. Elaboration using solar energy leads to obtaining pure and doped nanometric particles with dimensions smaller than 60 nm.

The crustal structure parameters space group, average crystallite size D (nm), cell parameters *a* and c (Å), cell volume V ($Å^3$), and unit cell volume *u* (Å) are also determined from XRD data (Table II).

The lattice parameters for commercial ZnO are 3.253 Å, 5.210Å, and 47.73Å3, respectively. The difference in lattice parameters of pure and doped ZnO nanostructured powders elaborated by solar energy is attributed to the strain induced by the nanoparticle's surface. The surface of a nanoparticle is curved, and this curvature creates a strain field that alters the bond lengths between atoms. As a result, the lattice parameters of ZnO nanoparticles are slightly smaller than those of bulk ZnO. This suggests that the crystal structure of pure and doped ZnO nanostructured powders is relatively robust and does not change significantly under solar synthesis conditions when solar flow varies, and the pressure is constant [35]. The smaller particle size of ZnO nanostructures allows more active sites for pollutant adsorption and decomposition, making them attractive for water, soil, and air purification applications. It can be deduced that the synthesis of ZnO pure and doped nanostructured powders is successfully achieved using concentrated solar energy in the solar reactor.

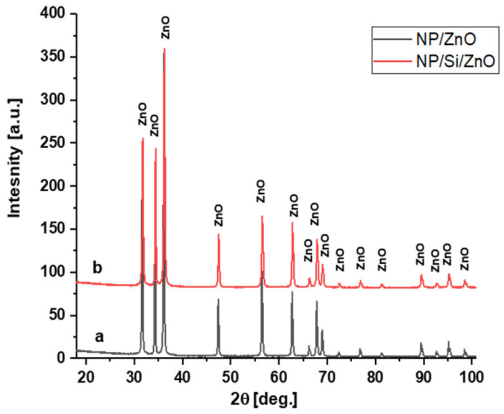

Fig. 3. XRD patterns of pure and Si-doped ZnO.

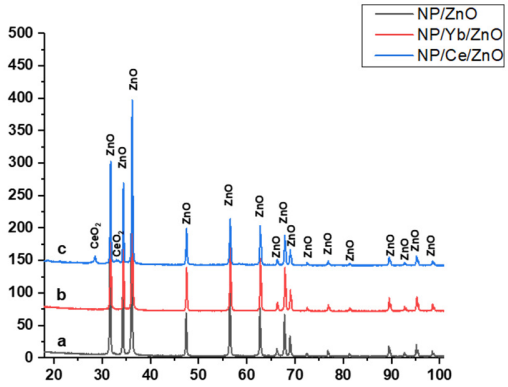

Fig. 4. XRD patterns of pure and Yb- and Ce-doped ZnO.

TABLE II. STRUCTURAL DATA FROM XRD PATTERNS

Sample	Phase	Space group	D (nm)	*a* (Å)	*c* (Å)	c/a	V ($Å^3$)	u (Å)
NP/ZnO	100% ZnO	186 : P63mc	51.16	3.2523	5.2106	1.6021	47.73	3.6274
NP/Mg/ZnO			44.14	3.2515	5.2093	1.6021	47.697	3.6266
NP/Fe/ZnO			47.94	3.2520	5.2105	1.6022	47.722	3.6272
NP/Si/ZnO			37.71	3.2517	5.2094	1.6021	47.703	3.6267
NP/Yb/ZnO			49.42	3.2517	5.2099	1.6022	47.708	3.6269
NP/Ce/ZnO	96.98% ZnO	186 : P63mc		3.2526	5.2109	1.6020	47.742	3.6277
	3.02% CeO_2	225 : Fm-3m		5.425	5.425	NA	159.66	5.4250

B. Morphological Characterization

Polyhedral ZnO nanoparticles are observed in micrometric powders, as shown in Figure 5. After solar radiation, the morphology of the nanoparticles is influenced by the method of concentrating solar energy, becoming pellets and whiskers, illustrated in Figure 6. The graphical representation of the distribution of particle sizes in ZnO micrometric particles exhibits a bimodal distribution while for ZnO nanoparticles is monomodal.

The morphology of Mg-ZnO doped powders from Figure 7 presents a nanorod form, densely packed together, with a length that varies between 0.18 and 1.1 µm. This micrograph

shows the highly crystalline and uniform nature of the Mg-doped ZnO nanoparticles elaborated with solar energy. The particle size histogram reveals that the most common length for Mg-ZnO doped nanoparticles lies between 0.38 and 0.61 µm.

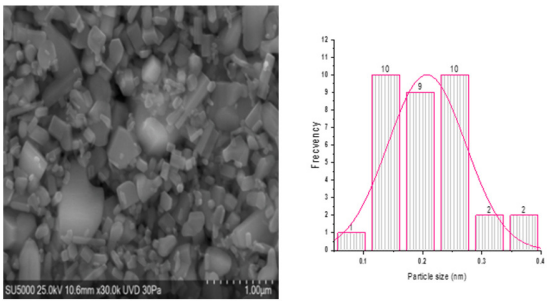

Fig. 5. SEM micrography of ZnO nanoparticle commercial powders and particle size histogram.

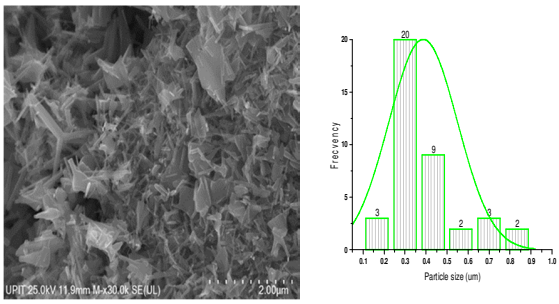

Fig. 6. SEM micrography of ZnO nanopowders and particle size histogram.

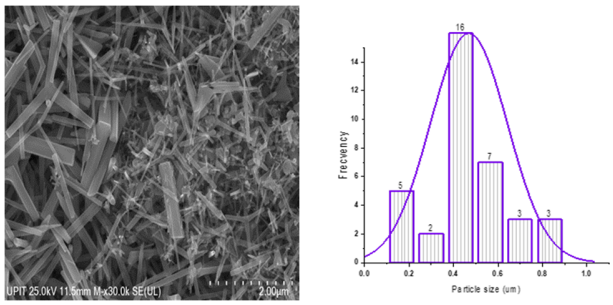

Fig. 7. SEM micrography and particle size histogram of NP/Mg/ZnO nanopowders.

Fe-doped ZnO nanoparticles have a specific morphology for synthesis with solar energy. Figure 8 highlights the formation of tetrapods with a uniform distribution of the length of the whiskers up to 1 µm. The same way of formation of tetrapods is also observed in Figure 9, in which the morphologies of the NP/Si/ZnO particles are presented. In addition to these, there are also a few almost spherical particles not totally elongated in tetrapods. Figure 10 demonstrates the uniform formation of tetrapod Yb-doped ZnO particles with elongated whiskers, characterized by lengths between 0.06 and 1.4 µm. The length size histogram presents a monomodal distribution. The morphologies change in the case of NP/Ce/ZnO due to the presence of the 2 phases ZnO and CeO_2. Figure 11 shows a mixture of spherical and tetrapodic morphologies.

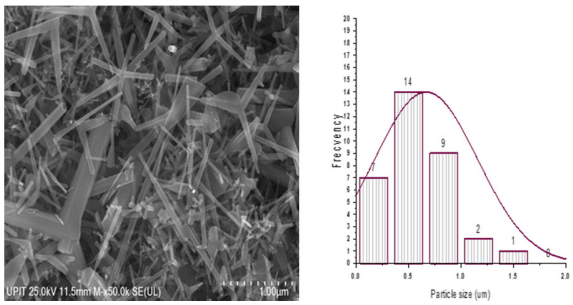

Fig. 8. SEM micrography and particle size histogram of NP/Fe/ZnO nanopowders.

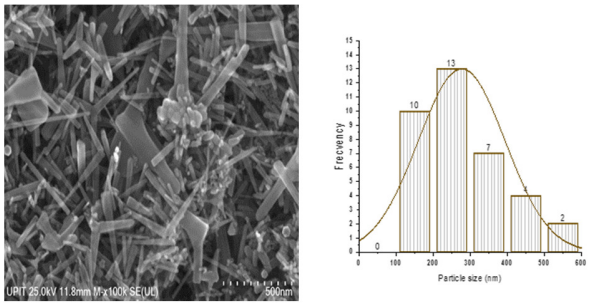

Fig. 9. SEM micrography and particle size histogram of NP/Si/ZnO nanopowders.

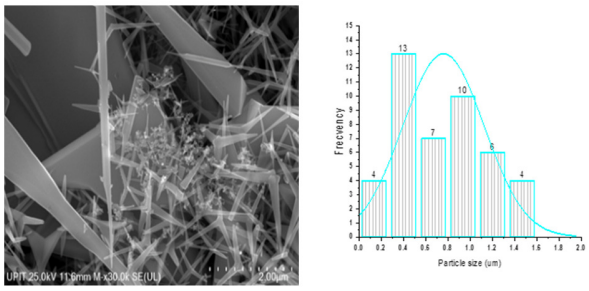

Fig. 10. SEM micrography and particle size histogram of NP/Yb/ZnO nanopowders.

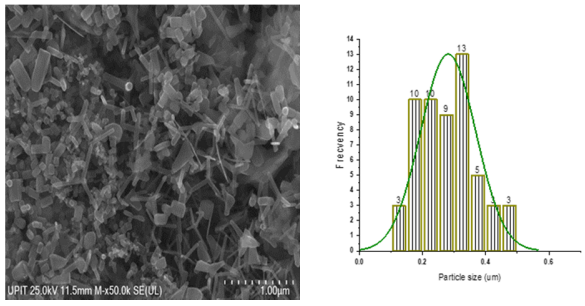

Fig. 11. SEM micrography and particle size histogram of NP/ce/ZnO nanopowders.

C. Surface Area

The surface area of nanoparticles, determined by BET method, and their lattice parameters are closely related. The specific surface area of the doped nanoparticles increases depending on the dopant element type, as shown in Table III. For dopants with a higher atomic radius the surface area increases accordingly. This trend can be explained by the fact that the atomic radius decreases from left to right across a period (Mg/160 pm; Fe/124 pm: Zn/133 pm; Si/114 pm; Ce/182 pm; Yb/160 pm). Also, the influence of lattice parameters on surface area is particularly evident in nanoparticles with high aspect ratios, such as nanowhiskers. These structures exhibit a large surface area due to their elongated shape and relatively small cross-sectional area.

TABLE III. SURFACE CHARACTERISTICS OF PURE AND DOPED ZnO NANOPARTICLES

Sample	Surface area (m^2/g)	Total pore volume (cm^3/g)	Nanoparticle average size (BET) nm	Max. pore volume (cm^3/g)
NP/ZnO	4.0618	0.003975	263.3127	0.002327
NP/Mg/ZnO	11.494	0.016832	93.0503	0.004769
NP/Fe/ZnO	12.5207	0.016345	85.4197	0.004530
NP/Si/ZnO	16.0099	0.026692	66.4331	0.005919
NP/Yb/ZnO	21.6544	0.025043	49.3903	0.005459
NP/Ce/ZnO	14.9353	0.020634	71.6102	0.004837

As the lattice parameters of pure and doped ZnO nanoparticles decrease (as shown in Table III), their surface area increases rapidly due to the large surface-to-volume ratio, because the atoms in the crystal lattice are packed more tightly together, which reduces the spacing between them and increases surface area. Smaller ZnO nanoparticles have a higher surface area and are more reactive. Additionally, the increased surface area allows for more efficient charge separation, which is essential for the photocatalytic process. Thus, ZnO nanostructures elaborated by solar energy can have enhanced photocatalytic activity compared to bulk ZnO. This increase in surface area can have a significant impact on the properties of nanoparticles, including their reactivity, catalytic activity, and optical properties [36].

D. Optical Characterization

Optical properties were determined for all developed nanoparticles. The UV-VIS spectra are shown in Figure 12. The Tauc plot method was used to energy bandgap determination. The Tauc plot is obtained by plotting the absorption coefficient vs. the square root of E (energy band gap). The bandgap was determined from the intercept of the linear fit with the absorption coefficient axis. The band gap of pure and doped ZnO nanopowders elaborated on solar reactor was determined by extrapolating the linear region of the energy gap from Figure 13. The determined energy gap of ZnO nanoparticles is typically 2.83 eV, depending on the size and morphology of the nanoparticles [39]. Doping ZnO with Mg and Si can slightly increase the band gap, resulting in a small blue shift of the absorption band. However, the effect is much smaller than for Fe doping. Doping ZnO with Fe increases the band gap at 3.14 eV, resulting in a small blue shift of the absorption band. This can be attributed to the formation of Fe-related defect states within the band gap, which emit more photons. Doping ZnO with Yb increases the band gap at 3.06 eV while doping ZnO with Ce grows the band gap at 3.00 eV, resulting in a small blue shift of the absorption band. Absorbance depends on the type of nanoparticle and corresponds to each dopant.

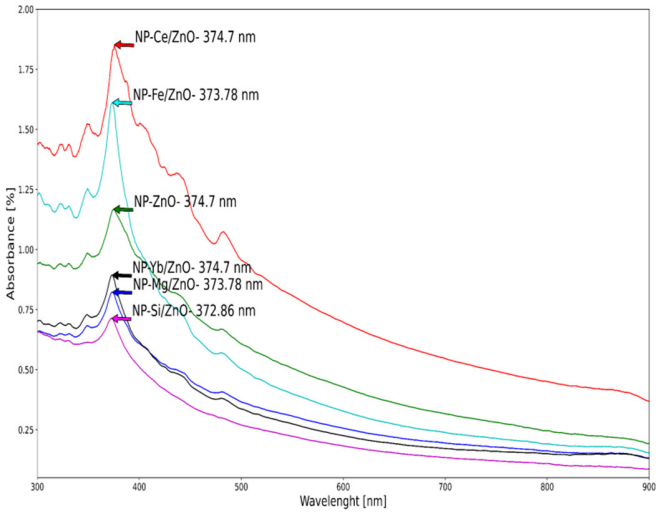

Fig. 12. UV-Vis spectra of pure and doped ZnO powders.

The values of optical energy, absorbance, and wavelengths, determined from the UV-VIS spectra, are summarized in Table IV.

TABLE IV. OPTICAL CHARACTERISTICS OF NP/ZNO

Sample	Eg (ev)	Wavelength (nm)	A max (%)	Dopant atomic radius (pm)
NP/ZnO	2.99	375.62	2.54	133
NP/Mg/ZnO	2.83	374.7	1.17	160
NP/Fe/ZnO	3.04	373.78	0.82	124
NP/Si/ZnO	3.14	373.78	1.61	114
NP/Yb/ZnO	3.02	372.86	0.71	160
NP/Ce/ZnO	3.06	373.32	0.89	182

A smaller lattice parameter of doped ZnO nanoparticles corresponds to a wider band gap, which means that solar elaborated nanoparticles absorb light at a shorter wavelength. When the ZnO particles become smaller, the quantum confinement restricts the movement of electrons between VB and CB, increasing the band gap. The surface effects and the elongated form of particles dominate the behavior. This can be beneficial for applications such as photocatalysis, where ZnO nanoparticles are used to break down organic molecules using light energy and for ultraviolet light detection [37-43]. The surface area and lattice parameters of solar synthesized ZnO nanoparticles are interconnected properties that have a profound impact on their overall properties. As research in this field continues to advance, we can expect to see even more innovative materials emerge, further propelling the growth of the solar energy industry.

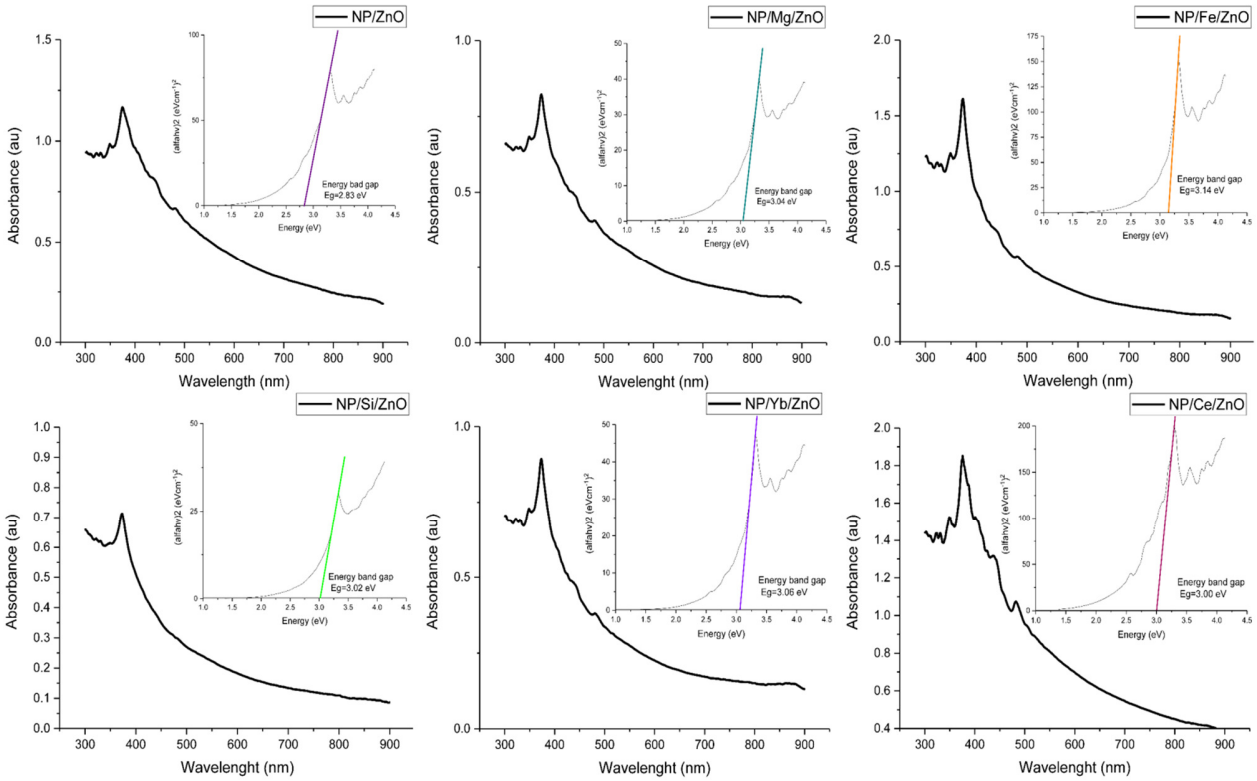

Fig. 13. Energy band gap spectra of pure and doped ZnO powders.

IV. CONCLUSIONS

Among all methods of ZnO nanoparticle elaboration, solar-evaporation offers advantages such as energy efficiency, environmental friendliness, and the ability to synthesize nano-oxides with tailored properties, making them promising approaches for sustainable nano-oxide production. The novelty of solar synthesis lies in its ability to address environmental concerns, reduce costs, enhance control over material properties, promote sustainable manufacturing practices, and enable the discovery of novel materials with transformative applications.

The tetrapod morphology (provided by SEM) of pure and doped ZnO nanometric particle (from XRD) synthesis by solar energy can significantly influence their properties and applications. For instance, these nanoparticles are suitable for gas sensors and field-effect transistors due to their high surface area (demonstrated by BET). Having a larger proportion of atoms or molecules on their surfaces leads to enhanced interactions with their surroundings. By analyzing the ATR-FTIR spectrum of Mg-, Fe-, Si-, Yb-, and Ce-doped ZnO nanoparticles, researchers can gain insights into the structural doping effects. Tetrapod type morphology observed to have been formed by solar synthesis exhibits unique optical properties demonstrated by UV-VIS analysis. Thus, we can state that these nano-oxides can be used in various sensing and photonic applications.

As solar energy becomes more accessible and efficient, solar-driven synthesis of pure and doped ZnO is poised to be a crucial factor in shaping the future of materials science and technology. Therefore, understanding and controlling the structure and morphology of ZnO nanoparticles is crucial for optimizing their performance in various applications.

ACKNOWLEDGMENT

This project has received funding from the European Union's Horizon 2020 Research and Innovation Program under grant agreement No 823802. We thank the CNRS-PROMES laboratory, UPR 8521, belonging to the French National Centre for Scientific Research (CNRS), for providing access to its installations, the support of its scientific and technical staff, and the financial support of the SFERA-III project (Grant Agreement No 823802). The characterization was supported by The National University of Science and Technology POLITEHNICA Bucharest, Pitești University Centre under grant agreement CIPCS-2022-6 (Enhance the efficiency of solar cells by coating with nanostructured metal oxide layers).

REFERENCES

[1] D. Tan, Y. Wu, Z. Zhang, Y. Jiao, L. Zeng, and Y. Meng, "Assessing the Life Cycle Sustainability of Solar Energy Production Systems: A Toolkit Review in the Context of Ensuring Environmental Performance Improvements," *Sustainability*, vol. 15, no. 15, Jan. 2023, Art. no. 11724, https://doi.org/10.3390/su151511724.

[2] S. Kuskaya, F. Bilgili, E. Mugaloglu, K. Khan, M. E. Hoque, and N. Toguc, "The role of solar energy usage in environmental sustainability: Fresh evidence through time-frequency analyses," *Renewable Energy*, vol. 206, pp. 858–871, Apr. 2023, https://doi.org/10.1016/j.renene.2023.02.063.

[3] N. Novas, R. M. Garcia, J. M. Camacho, and A. Alcayde, "Advances in Solar Energy towards Efficient and Sustainable Energy," *Sustainability*,

vol. 13, no. 11, Jan. 2021, Art. no. 6295, https://doi.org/10.3390/su13116295.

[4] G. I. Mamniashvili, G. Donadze, V. Tavkhelidze, and D. Gulamova, "Superconducting Precursors in Bi/Pb Multiphase Cuprates Fabricated by the Solar Technology and their Comparative Study by Torque Magnetometry Methods," *Engineering, Technology & Applied Science Research*, vol. 13, no. 6, pp. 12390–12395, Dec. 2023, https://doi.org/10.48084/etasr.6487.

[5] N. S. M. N. Izam, Z. Itam, W. L. Sing, and A. Syamsir, "Sustainable Development Perspectives of Solar Energy Technologies with Focus on Solar Photovoltaic—A Review," *Energies*, vol. 15, no. 8, Jan. 2022, Art. no. 2790, https://doi.org/10.3390/en15082790.

[6] M. Oelgemoller, "Solar Photochemical Synthesis: From the Beginnings of Organic Photochemistry to the Solar Manufacturing of Commodity Chemicals," *Chemical Reviews*, vol. 116, no. 17, pp. 9664–9682, Sep. 2016, https://doi.org/10.1021/acs.chemrev.5b00720.

[7] L. G. Ceballos-Mendivil, Y. Carvajal-Campos, J. Tanori-Cordova, J. C. Luque-Ceballos, H. Villafan-Vidales, and C. A. Estrada, "Solar synthesis of nanostructured zirconia: microstructural and thermal characterization," *Materials Research Express*, vol. 7, no. 11, Aug. 2020, Art. no. 115014, https://doi.org/10.1088/2053-1591/abcbb8.

[8] N. Shohoji, L. Guerra Rosa, J. Cruz Fernandes, D. Martinez, and J. Rodriguez, "Catalytic acceleration of graphitisation of amorphous carbon during synthesis of tungsten carbide from tungsten and excess amorphous carbon in a solar furnace," *Materials Chemistry and Physics*, vol. 58, no. 2, pp. 172–176, Mar. 1999, https://doi.org/10.1016/S0254-0584(98)00275-2.

[9] K. K. Brar *et al.*, "Green route for recycling of low-cost waste resources for the biosynthesis of nanoparticles (NPs) and nanomaterials (NMs)-A review," *Environmental Research*, vol. 207, May 2022, Art. no. 112202, https://doi.org/10.1016/j.envres.2021.112202.

[10] N. Shohoji *et al.*, "Synthesising Carbo-Nitrides of some D-Group Transition Metals Using a Solar Furnace at PSA," *Materials Science Forum*, vol. 730–732, pp. 153–158, 2013, https://doi.org/10.4028/www.scientific.net/MSF.730-732.153.

[11] G. Flamant, A. Ferriere, D. Laplaze, and C. Monty, "Solar processing of materials: opportunities and new frontiers," *Solar Energy*, vol. 66, no. 2, pp. 117–132, Jun. 1999, https://doi.org/10.1016/S0038-092X(98)00112-1.

[12] R. Roman, I. Canadas, J. Rodriguez, M. T. Hernandez, and M. Gonzalez, "Solar sintering of alumina ceramics: Microstructural development," *Solar Energy*, vol. 82, no. 10, pp. 893–902, Oct. 2008, https://doi.org/10.1016/j.solener.2008.04.002.

[13] Z. H. Wang, C. J. Choi, B. K. Kim, J. C. Kim, and Z. D. Zhang, "Characterization and magnetic properties of carbon-coated cobalt nanocapsules synthesized by the chemical vapor-condensation process," *Carbon*, vol. 41, no. 9, pp. 1751–1758, Jan. 2003, https://doi.org/10.1016/S0008-6223(03)00127-1.

[14] J. Ahire and B. M. Bhanage, "Solar energy-controlled shape selective synthesis of zinc oxide nanomaterials and its catalytic application in synthesis of glycerol carbonate," *Journal of Solid State Chemistry*, vol. 295, Mar. 2021, Art. no. 121927, https://doi.org/10.1016/j.jssc.2020.121927.

[15] D. D. Dionysiou, S. C. Pillai, and S. Rtimi, "Editorial overview: Nanomaterials for energy and environmental applications: advances and recent trends," *Current Opinion in Chemical Engineering*, vol. 36, Jun. 2022, Art. no. 100805, https://doi.org/10.1016/j.coche.2022.100805.

[16] Y. Zhang, K. Poon, G. S. P. Masonsong, Y. Ramaswamy, and G. Singh, "Sustainable Nanomaterials for Biomedical Applications," *Pharmaceutics*, vol. 15, no. 3, Mar. 2023, Art. no. 922, https://doi.org/10.3390/pharmaceutics15030922.

[17] M. Parashar, V. K. Shukla, and R. Singh, "Metal oxides nanoparticles via sol–gel method: a review on synthesis, characterization and applications," *Journal of Materials Science: Materials in Electronics*, vol. 31, no. 5, pp. 3729–3749, Mar. 2020, https://doi.org/10.1007/s10854-020-02994-8.

[18] A. G. Plaiasu, C. M. Topala, A. Dinu, C. Sutan, and M. Abrudeanu, "Copper oxides nanopowders: Synthesis by S.P.V.D. And characterization," *Revista de Chimie*, vol. 66, no. 10, pp. 1636–1638, Oct. 2015.

[19] W. Jiang *et al.*, "Preparation and properties of superparamagnetic nanoparticles with narrow size distribution and biocompatible," *Journal of Magnetism and Magnetic Materials*, vol. 283, no. 2, pp. 210–214, Dec. 2004, https://doi.org/10.1016/j.jmmm.2004.05.022.

[20] Z. Sadowski and A. Pawlowska, "Synthesis of Metal Oxide Nanoparticles and Its Biomedical Applications," in *Nanotechnology Applied To Pharmaceutical Technology*, M. Rai and C. Alves dos Santos, Eds. New York, NY, USA: Springer, 2017, pp. 91–111.

[21] L. M. Cursaru, A. G. Plaiasu, C. M. Ducu, R. M. Piticescu, and I. A. Tudor, "Carbon Nanotube/Polyaniline Composite Films Prepared by Hydrothermal- Electrochemical Method for Biosensor Applications," in *International Semiconductor Conference*, Sinaia, Romania, Oct. 2018, pp. 249–252, https://doi.org/10.1109/SMICND.2018.8539793.

[22] J. Jeevanandam *et al.*, "Green approaches for the synthesis of metal and metal oxide nanoparticles using microbial and plant extracts," *Nanoscale*, vol. 14, no. 7, pp. 2534–2571, Feb. 2022, https://doi.org/10.1039/D1NR08144F.

[23] M.-A. Iota, L.-M. Cursaru, A.-G. Schiopu, I. A. Tudor, A.-M. Motoc, and R. M. Piticescu, "Fe3O4 Core–Shell Nanostructures with Anticancer and Antibacterial Properties: A Mini-Review," *Processes*, vol. 11, no. 7, Jul. 2023, Art. no. 1882, https://doi.org/10.3390/pr11071882.

[24] L. Yan, A. Uddin, and H. Wang, "ZnO Tetrapods: Synthesis and Applications in Solar Cells," *Nanomaterials and Nanotechnology*, vol. 5, Jan. 2015, Art. no. 19, https://doi.org/10.5772/60939.

[25] N. A. Hussien, J. S. Al Malki, F. A. R. Al Harthy, A. W. Mazi, and J. A. A. Al Shadadi, "Sustainable Eco-Friendly Synthesis of Zinc Oxide Nanoparticles Using Banana Peel and Date Seed Extracts, Characterization, and Cytotoxicity Evaluation," *Sustainability*, vol. 15, no. 13, Jan. 2023, Art. no. 9864, https://doi.org/10.3390/su15139864.

[26] A. C. Constandache *et al.*, "Morphological and structural investigations of ZnO resulted from green synthesis," *Scientific Bulletin-University Politehnica of Bucharest*, vol. 85, no. 2, pp. 275–283, 2023.

[27] A. Mir, N. Becheikh, L. Khezami, M. Bououdina, and A. Ouderni, "Synthesis, Characterization, and Study of the Photocatalytic Activity upon Polymeric-Surface Modification of ZnO Nanoparticles," *Engineering, Technology & Applied Science Research*, vol. 13, no. 6, pp. 12047–12053, Dec. 2023, https://doi.org/10.48084/etasr.6373.

[28] E. Guillot, R. Rodriguez, N. Boullet, and J.-L. Sans, "Some details about the third rejuvenation of the 1000 kWth solar furnace in Odeillo: Extreme performance heliostats," *AIP Conference Proceedings*, vol. 2033, no. 1, Nov. 2018, Art. no. 040016, https://doi.org/10.1063/1.5067052.

[29] M. Quiros, S. Grazulis, S. Girdzijauskaite, A. Merkys, and A. Vaitkus, "Using SMILES strings for the description of chemical connectivity in the Crystallography Open Database," *Journal of Cheminformatics*, vol. 10, no. 1, May 2018, Art. no. 23, https://doi.org/10.1186/s13321-018-0279-6.

[30] A. Merkys, A. Vaitkus, J. Butkus, M. Okulic-Kazarinas, V. Kairys, and S. Grazulis, "COD::CIF::Parser: an error-correcting CIF parser for the Perl language," *Journal of Applied Crystallography*, vol. 49, no. 1, pp. 292–301, Feb. 2016, https://doi.org/10.1107/S1600576715022396.

[31] S. Grazulis, A. Merkys, A. Vaitkus, and M. Okulic-Kazarinas, "Computing stoichiometric molecular composition from crystal structures," *Journal of Applied Crystallography*, vol. 48, no. 1, pp. 85–91, Feb. 2015, https://doi.org/10.1107/S1600576714025904.

[32] S. Grazulis *et al.*, "Crystallography Open Database (COD): an open-access collection of crystal structures and platform for world-wide collaboration," *Nucleic Acids Research*, vol. 40, no. D1, pp. D420–D427, Jan. 2012, https://doi.org/10.1093/nar/gkr900.

[33] S. Grazulis *et al.*, "Crystallography Open Database – an open-access collection of crystal structures," *Journal of Applied Crystallography*, vol. 42, no. 4, pp. 726–729, Aug. 2009, https://doi.org/10.1107/S0021889809016690.

[34] R. T. Downs and M. Hall-Wallace, "The American Mineralogist crystal structure database," *American Mineralogist*, vol. 88, no. 1, pp. 247–250, Jan. 2003.

[35] N. L. Nguyen and N. N. Ha, "Understanding ZnO surface defects from first-principles simulation," *Surface Science*, vol. 732, Jun. 2023, Art. no. 122272, https://doi.org/10.1016/j.susc.2023.122272.

[36] M. M. Nadareishvili, G. Mamniashvili, D. Jishiashvili, G. Abramishvili, C. Ramana, and J. Ramsden, "Investigation of the Visible Light-Sensitive ZnO Photocatalytic Thin Films," *Engineering, Technology & Applied Science Research*, vol. 10, no. 2, pp. 5524–5527, Apr. 2020, https://doi.org/10.48084/etasr.3392.

[37] H. M. Pouran, F. L. Martin, and H. Zhang, "Measurement of ZnO Nanoparticles Using Diffusive Gradients in Thin Films: Binding and Diffusional Characteristics," *Analytical Chemistry*, vol. 86, no. 12, pp. 5906–5913, Jun. 2014, https://doi.org/10.1021/ac500730s.

[38] T. M. Awwad, S. M. Shaaban, E. M. Ragab, and A. Mir, "Photo-Catalytic Activity Improvement for Organic Pollutant Removal in Wastewater using Zinc Oxide Quantum Dots: An Experimental and Modeling Study," *Engineering, Technology & Applied Science Research*, vol. 13, no. 6, pp. 12138–12144, Dec. 2023, https://doi.org/10.48084/etasr.6451.

[39] C. Wang, Z. Chen, Y. He, L. Li, and D. Zhang, "Structure, morphology and properties of Fe-doped ZnO films prepared by facing-target magnetron sputtering system," *Applied Surface Science*, vol. 255, no. 15, pp. 6881–6887, May 2009, https://doi.org/10.1016/j.apsusc.2009.03.008.

[40] K. Kaviyarasu, X. Fuku, G. T. Mola, E. Manikandan, J. Kennedy, and M. Maaza, "Photoluminescence of well-aligned ZnO doped CeO2 nanoplatelets by a solvothermal route," *Materials Letters*, vol. 183, pp. 351–354, Nov. 2016, https://doi.org/10.1016/j.matlet.2016.07.143.

[41] S. K. Noukelag *et al.*, "Investigation of structural and optical properties of biosynthesized Zincite (ZnO) nanoparticles (NPs) via an aqueous extract of Rosmarinus officinalis (rosemary) leaves," *MRS Advances*, vol. 5, no. 45, pp. 2349–2358, Jan. 2020, https://doi.org/10.1557/adv.2020.220.

[42] S. K. Dhoke, "Synthesis of nano-ZnO by chemical method and its characterization," *Results in Chemistry*, vol. 5, Jan. 2023, Art. no. 100771, https://doi.org/10.1016/j.rechem.2023.100771.

[43] A. Anzlovar, Z. Crnjak Orel, and M. Zigon, "Nanocomposites with nano-to-sub-micrometer size zinc oxide as an effective UV absorber," *Polimeri : casopis za plastiku i gumu*, vol. 29, no. 2, pp. 84–87, Nov. 2008.